Magnetometer Calibration Using Kalman Filter Covariance Matrix for Online Estimation of Magnetic Field Orientation

Tadej Beravs, Samo Beguš, Janez Podobnik, and Marko Munih, *Member, IEEE*

***Abstract*— The inertial/magnetic measurement units are an affordable instrument for the determination of orientation. The sensors embedded in the system are affected by nonidealities that can be greatly compensated by proper calibration, by determining sensor parameters, such as bias, misalignment, and sensitivity/gain. This paper presents an online calibration method for a three-axial magnetometer using a 3-D Helmholtz coil. The magnetometer is exposed to different directions of the magnetic field created by the 3-D coil. The parameters are estimated by using an unscented Kalman filter. The directions are calculated online by using a sensor parameter covariance matrix. The method evaluation is achieved by first running numerous simulations, followed by experiments using a real magnetometer, finally resulting in better accuracy of parameter estimation with a low number of measurement iterations compared with the method where magnetic field directions are determined manually.**

***Index Terms*— Magnetometer calibration, orientation determination, sensor parameter estimation, unscented Kalman filtering (UKF).**

I. Introduction

THE applicability of inertial/magnetic measurement units is increasing, as they represent an inexpensive and lightweight instrument for orientation estimation compared with more sophisticated optical measurement systems [1]. Inertial/magnetic measurement systems can be found in navigation systems [2], robotics [3], and in applications for estimating human body kinematics [4]. In general, the inertial measurement unit system consists of a gyroscope, accelerometer, and in some cases also a magnetometer, and can deliver good dynamics specifications with a relatively low investment. However, the implementation of an inexpensive sensor results in numerous disadvantages, such as sensor misalignment, large offsets, nonlinearity, drift, and random noise.

In general, the estimation of orientation is derived from the gyroscope during dynamic movements and the correction of orientation is derived from the accelerometer and magnetometer while the sensor is stationary using different mathematical algorithms [5]. It is therefore important that the outputs from the accelerometer and magnetometer are accurate, which can be achieved by correct sensor calibration.

Both the accelerometer and magnetometer can be calibrated using the same calibration methods since the basic principles of the sensors are the same. However, the accelerometer has an advantage since the magnitude and orientation of the gravitational field is constant regardless of the position of the sensor. The only condition that must be met during calibration is that the sensor must be stationary during the measurement. The homogeneity of the magnetic field, especially inside buildings, where electromagnetic noise is unavoidable, is hard to achieve. Large ferromagnetic materials inside the floors and walls, and moving metal objects, such as elevators, contradict the assumption that the magnetic field has a constant orientation and amplitude. However, if the indoor magnetic field stays constant it can be used for the calibration, even with the presence of magnetic perturbations.

These disadvantages are generally addressed by using a sensor calibration method. The calibration can be done by using different mathematical approaches that estimates parameters either offline or online. A comprehensive list of offline calibration methods can be found in [6]. The numerical calibration method for estimating sensor parameters requires several different sensor orientations set manually as described in [7]. The parameters are determined by using the Levenberg–Marquardt algorithm. A similar algorithm is used in [8], where the parameters are determined by using Newton iterative arithmetic. A procedure for estimating sensor parameters using the least-mean square method is presented in [9], where a large set of measurements is required. To obtain a large set of measurements, different types of equipment can be used to perform the calibration. This can be done by either moving the sensor in a constant magnetic field or by keeping the sensor in fixed orientation or changing the direction of magnetic field. A method that use a sophisticated equipment is described in [10], where the magnetometer is placed in different orientations using a custom-designed platform equipped with sensors, which measure the orientation of the platform. A method where a robot arm is used to position the sensor to a known predefined orientation is presented in [11], where the parameters of the sensor are again determined using the least-mean square method. In [12], a precise setup of a 3-D Helmholtz coil is used for calibration. However, since several of the factors that contribute to sensor errors are time-varying (e.g., temperature), initial offline calibration cannot completely negate their effects. Thus, an online cal-

Manuscript received May 27, 2013; revised September 27, 2013; accepted November 17, 2013. The Associate Editor coordinating the review process was Dr. Salvatore Baglio. This work was funded by the European Union Collaborative Project CareToy grant FP7-ICT-287932, the European Union Collaborative Project CYBERLEGs grant FP7-ICT-287894 and additionally supported by the Slovenian Research Agency (ARRS).

T. Beravs, J. Podobnik and M. Munih are with the Laboratory of Robotics, Faculty of Electrical Engineering, University of Ljubljana, Ljubljana 1000, Slovenia (e-mail: tadej.beravs@robo.fe.uni-lj.si).

S. Begus is with the Laboratory of Metrology and Quality, Faculty of Electrical Engineering, University of Ljubljana, Ljubljana 1000, Slovenia.

Color versions of one or more of the figures in this paper are available online at http://ieeexplore.ieee.org.

Digital Object Identifier 10.1109/TIM.2014.2302240

ibration procedure could potentially achieve higher accuracy. Online approaches have already been demonstrated in [13] and [14], but the different sensor orientations needed for the calibration must be predefined in both cases. These methods require a manual determination of the appropriate orientations of the sensor where a misalignment of the sensor can result in a lower accuracy of the sensor parameters, or a large number of random orientations must be acquired to accomplish an accurate calibration resulting in a time-consuming task.

This paper presents an automatic calibration method of the magnetometer, where the parameters and orientations of the magnetic field are estimated by an unscented Kalman filter (UKF). A 3-D Helmholtz coil is used to create a magnetic field in the estimated orientation. The method is used to determine three parameters of gain, misalignment, and bias together with the alignment angles of the coil (since the reference magnetometer and sensor board are not perfectly aligned). The proposed method repeatedly uses the covariance matrix decomposition for the estimation of the maximal sensitivity axis to assess the next best orientation of the magnetic field that the sensor should be exposed to for optimal parameter estimation, taking into account maximal sensitivity. This results in a fast method convergence. The sensor is thus exposed to a small number of automatically determined orientations of the magnetic field, eliminating the need for a large number of predefined orientations, which leads to a faster calibration procedure.

This paper is organized as follows. The hardware setup of the calibration system and the corresponding mathematical model of the sensor system in conjunction with the 3-D Helmholtz coil is described in the first part of Section II. Parameter estimation based on the UKF is described together with the method for determining the magnetic field orientation using singular value decomposition (SVD) in the second part of Section II. The simulation and measurement procedures are described at the end of the section. The simulation and measurement results are presented in Section III, and a detailed discussion is given in Section IV. Section V summarizes the proposed calibration method and the contributions of this paper.

II. Method

A. Hardware Design

The 3-D magnetometer that is subject of the calibration is part of a wireless battery-powered inertial measurement system also consisting of a 3-D accelerometer and a 3-D gyroscope [15]. Data acquisition from all three sensors is carried out with a frequency of 100 Hz, and the data are sent wirelessly to a personal computer. Since the ferromagnetic materials embedded in the battery interfere with the magnetic field, the battery must be placed away from the sensor during the calibration.

The wireless inertial measurement system is placed on a plastic platform in the center of a 3-D Helmholtz coil as shown in Fig. 1. The 3-D Helmholtz coil consists of three perpendicular placed pairs of coils [16]. The coils are current driven and can be used in conjunction with an analog or digital

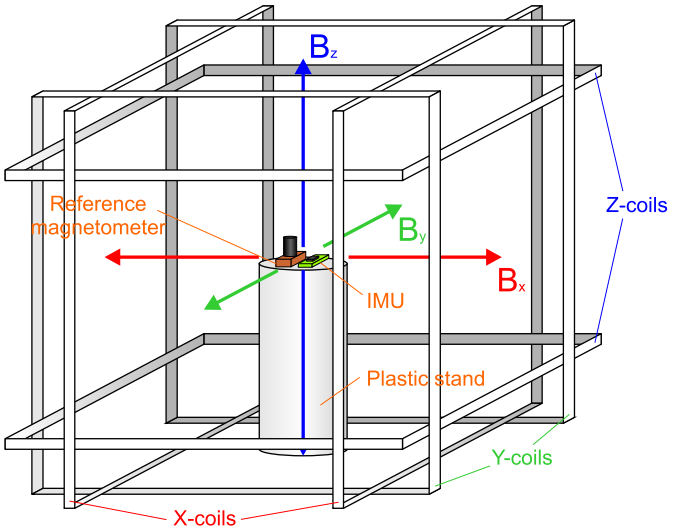

Fig. 1. Illustration shows the 3-D Helmholtz coil. The axes B_x, B_y, and B_z represent the components of the magnetic field generated by each coil pair. Inside the center of the coil is a plastic stand on which the reference and calibrated magnetometer are placed.

controller. By controlling the current that runs through the coils, we can generate a magnetic field in any direction in the center of the 3-D coil as shown in (1). The maximal amplitude of the magnetic field in any direction is 0.1 mT

$$\mathbf{B} = B_x \cdot \mathbf{i} + B_y \cdot \mathbf{j} + B_z \cdot \mathbf{k} = \mathbf{B}_x + \mathbf{B}_y + \mathbf{B}_z. \tag{1}$$

With the appropriate analog controller, the coil is able to compensate the magnetic field for the earth as well as 50-Hz electromagnetic interferences and other magnetic disturbances. For control purposes, the reference 3-D magnetometer is also placed in the center of the coil. Since the desired direction of the magnetic field is computer calculated, the coils need to be computer driven. Thus, the digital controller is implemented in such a way that it is able to compensate for the magnetic field of the earth and other slowly changing magnetic disturbances. However, due to the slower refresh rate of the digital controller, the 3-D Helmholtz coil is not able to compensate for 50-Hz electromagnetic interferences.

B. Kinematic Model of the Sensor

A basic mathematical model of a three-axis magnetometer that includes gain, misalignment, and bias parameters can be described as

$$\mathbf{y} = \mathbf{s} \cdot \mathbf{T} \cdot \mathbf{u} + \mathbf{b} + N \tag{2}$$

where vector $\mathbf{y}$ represents the output of the sensor in x, y, and z axes direction, matrix $\mathbf{s} = \text{diag}([\, s_x \;\; s_y \;\; s_z \,])$ denotes the scaling factor of the each axis, matrix $\mathbf{T}$ is described as

$$\mathbf{T} = \begin{bmatrix} 1 & 0 & 0 \\ \cos\alpha & 1 & 0 \\ \cos\beta & \cos\gamma & 1 \end{bmatrix} \tag{3}$$

where α, β, and γ represent misalignment angles, vector $\mathbf{b} = [b_x \;\; b_y \;\; b_z]^{\mathrm{T}}$ denotes the bias, N represents the noise, and

vector $\mathbf{u} = [u_x\ u_y\ u_z]^{\mathrm{T}}$ denotes the magnetic field projection on the sensor axes [17].

The 3-D Helmholtz magnetic coil with the appropriate control system is capable of compensating for outer magnetic field and produces a magnetic field in an arbitrary direction. The reference magnetometer that is used to control the coil is placed on the same plane as the magnetometer to be calibrated; however, due to the casing of the magnetometer, misalignment can occur. A transformation matrix between the orientation of the reference magnetic field and the orientation of the magnetometer to be calibrated must therefore be considered. The transformation matrix can be described as

$$\mathbf{R}_{\mathrm{r\_m}} = \mathrm{Rot}Z(\varphi_z) \cdot \mathrm{Rot}X(\varphi_x) \tag{4}$$

where φ_x and φ_z denote the rotation angles around the x and z axes in the coordinate system of the reference magnetometer. The functions Rot$Z$ and Rot$X$ are determined as follows:

$$\mathrm{Rot}X = \begin{bmatrix} 1 & 0 & 0 \\ 0 & \cos\varphi_x & -\sin\varphi_x \\ 0 & \sin\varphi_x & \cos\varphi_x \end{bmatrix} \tag{5}$$

$$\mathrm{Rot}Z = \begin{bmatrix} \cos\varphi_z & -\sin\varphi_z & 0 \\ \sin\varphi_z & \cos\varphi_z & 0 \\ 0 & 0 & 1 \end{bmatrix}. \tag{6}$$

With both orientational matrices known, a transformation between the reference magnetic field and the real projection of the magnetic field on the sensor $\mathbf{u}$ can be calculated by

$$\mathbf{u} = \mathbf{R}_{\mathrm{r\_m}} \cdot \mathbf{B}. \tag{7}$$

With the transformation matrix specified, the output $\mathbf{y}$ of the magnetometer can be described as

$$\mathbf{y} = \mathbf{s} \cdot \mathbf{T} \cdot \mathbf{R}_{\mathrm{r\_m}}^{-1} \cdot \mathbf{B} + \mathbf{b} + N. \tag{8}$$

C. Magnetometer Parameter Estimation

The UKF is an extension of the traditional Kalman filter for the estimation of nonlinear systems that attempts to remove some of the shortcomings of the extended Kalman filter in the estimation of nonlinear systems [18]–[20]. The UKF uses deterministic sampling to approximate the state distribution. The unscented transformation uses a set of samples, or sigma points that are determined from the *a priori* mean and covariance of the state. The sigma points are then propagated through the nonlinear system. The posterior mean and covariance are then calculated from the propagated sigma points. The parameter estimation equations for the UKF are similar to those for state estimation. This section expounds upon the differences. A detailed description of parameter estimation using the UKF filter for a similar mathematical model is presented in [21].

The filter is initialized with the initial mean and covariance of the parameters

$$\hat{\mathbf{w}}(t_0) = E\{\mathbf{w}\} \tag{9}$$

$$\mathbf{P}_{\hat{\mathbf{w}}_0} = E\big\{(\mathbf{w}(t_0) - \hat{\mathbf{w}}_0)(\mathbf{w}(t_0) - \hat{\mathbf{w}}_0)^{\mathrm{T}}\big\} \tag{10}$$

where $E\{\}$ is the expectation operator, $(\mathbf{w} - \hat{\mathbf{w}}_0)$ is the estimation error of initial value, $\mathbf{w}$ is the unknown true parameter, and $\hat{\mathbf{w}}_0$ is the estimated initial parameter value. The UKF time-update is given by

$$\hat{\mathbf{w}}_k^- = \hat{\mathbf{w}}_{k-1} \tag{11}$$

$$\hat{\mathbf{P}}_{\mathbf{w}_k}^- = \mathbf{P}_{\mathbf{w}_{k-1}} + \eta_k \mathbf{R}_{\mathbf{w}_k} \tag{12}$$

where parameter vector $\mathbf{w}_k = [s_x\ s_y\ s_z\ \alpha\ \beta\ \gamma\ b_x\ b_y\ b_z\ \varphi_x\ \varphi_z]$ is updated using previous values, $\mathbf{R}_{\mathbf{w}_k}$ is the process noise diagonal matrix, and the $\hat{\mathbf{P}}_{\mathbf{w}_k}^-$ is the covariance matrix. Calculation of the covariance matrix $\hat{\mathbf{P}}_{\mathbf{w}_k}^-$ is based on recursive least-squares algorithm [18], [22] and is the sum of the covariance matrix from the previous step and $\mathbf{R}_{\mathbf{w}_k}$ matrix, which is annealed toward zero during the estimation of parameters. The decay parameter η_k is $\eta_k = \lambda^k$, where $\lambda \in (0,1]$ is a forgetting factor. The sigma points $\boldsymbol{\chi}_k$ are calculated from the values of the mean and covariance of the parameters

$$\boldsymbol{\chi}_{k|k-1} = \Big[\ \hat{\mathbf{w}}_k^- \quad \hat{\mathbf{w}}_k^- + \delta\sqrt{\hat{\mathbf{P}}_{\mathbf{w}_k}^-}\ \ \hat{\mathbf{w}}_k^- - \delta\sqrt{\hat{\mathbf{P}}_{\mathbf{w}_k}^-}\ \Big] \tag{13}$$

where $\delta = \sqrt{L + \lambda}$ is the proportion of the dispersion of the sigma point from the $\overline{\mathbf{x}}$. The expected measurement values are determined by the vector $\boldsymbol{\mathcal{Y}}$, by using the nonlinear sensor model denoted by $\mathbf{h}$ described earlier by (8)

$$\boldsymbol{\mathcal{Y}}_{k|k-1} = \mathbf{h}(\mathbf{x}_k, \boldsymbol{\chi}_{k|k-1}). \tag{14}$$

The measurement mean, $\hat{\mathbf{d}}_k^-$, and the measurement covariance, $\mathbf{P}_{\tilde{\mathbf{d}}_k}$, are calculated based on the statistics of the expected measurements

$$\hat{\mathbf{d}}_k^- = \sum_{i=0}^{2L} {w_i}^m \boldsymbol{\mathcal{Y}}_{i,k|k-1} \tag{15}$$

$$\mathbf{P}_{\tilde{\mathbf{d}}_k} = \sum_{i=0}^{2L} {w_i}^c \big(\boldsymbol{\mathcal{Y}}_{i,k|k-1} - \hat{\mathbf{d}}_k^-\big)\big(\boldsymbol{\mathcal{Y}}_{i,k|k-1} - \hat{\mathbf{d}}_k^-\big)^{\mathrm{T}} + \mathbf{R}_{\mathbf{e}_k}. \tag{16}$$

The weights ${w_i}^{(c)}$ and ${w_i}^{(m)}$ are calculated by equations described in [18].

The cross-correlation covariance, $\mathbf{P}_{\mathbf{w}_k\mathbf{d}_k}$, is calculated using

$$\mathbf{P}_{\mathbf{w}_k\mathbf{d}_k} = \sum_{i=0}^{2L} {w_i}^c \big(\boldsymbol{\chi}_{i,k|k-1} - \hat{\mathbf{w}}_k^-\big)\big(\boldsymbol{\mathcal{Y}}_{i,k|k-1} - \hat{\mathbf{d}}_k^-\big)^{\mathrm{T}}. \tag{17}$$

The Kalman gain matrix is a product of the cross-correlation and the measurement covariances

$$\mathbf{K}_k = \mathbf{P}_{\mathbf{w}_k\mathbf{d}_k} \mathbf{P}_{\tilde{\mathbf{d}}_k}^{-1}. \tag{18}$$

The measurement update equations are as follows:

$$\tilde{\mathbf{w}}_k = \hat{\mathbf{w}}_k^- + \mathbf{K}_k\big(\mathbf{d}_k - \hat{\mathbf{d}}_k^-\big) \tag{19}$$

$$\mathbf{P}_{\mathbf{w}_k} = \mathbf{P}_{\tilde{\mathbf{w}}_k} - \mathbf{K}_k \mathbf{P}_{\tilde{\mathbf{d}}_k} \mathbf{K}_k^{\mathrm{T}} \tag{20}$$

where current measurement is denoted as $\mathbf{d}_k$.

D. Determination of Magnetic Field Orientation

During the parameter estimation, the sensor must be subjected to several different orientations of the magnetic field to acquire an appropriate set of measurements for successful parameter estimation. In the proposed calibration algorithm, each subsequent orientation of the magnetic field is chosen in a direction in which maximal sensitivity is achieved for the parameters with the largest variance. This orientation can be determined from the covariance matrix $\mathbf{P}_{\tilde{\mathbf{d}}_k}$. The variance of parameters is described by the sigma points $\chi_{k|k-1}$, which are then propagated through the measurement model $\mathbf{h}$ (14). The outputs are transformed sigma points $\mathcal{Y}_{k|k-1}$, which capture the variance of parameters transformed from parameter space into cartesian space. This is needed to properly calculate the next orientation of the magnetic field, since it needs to be defined in cartesian space. The SVD algorithm is applied to covariance matrix $\mathbf{P}_{\tilde{\mathbf{d}}_k}$ [6]. Since a covariance $\mathbf{P}_{\tilde{\mathbf{d}}_k}$ is a positive semidefinite and symmetric matrix the following decomposition is obtained:

$$\mathrm{SVD}(\mathbf{P}_{\tilde{\mathbf{d}}_k}) = \mathbf{U} \cdot \Sigma \cdot \mathbf{U}^{\mathrm{T}}. \tag{21}$$

The $\mathbf{U} = [\mathbf{u}_1\ \mathbf{u}_2\ \mathbf{u}_3]$ is an orthogonal matrix of singular vectors and matrix Σ is a diagonal matrix of singular values $[\sigma_1\ \sigma_2\ \sigma_3]$. Singular values are associated with the variance. The singular value σ_1 is associated with the highest variance and thus, a unit vector $\mathbf{u}_1$ corresponds to the principle axis with the highest variance of the covariance matrix.

An intuitive interpretation of the proposed SVD approach is given by the principal component analysis (PCA) technique. The PCA uses an orthogonal transformation to transform the original space into a new one where the first axis points in the direction of the maximum variance, and the subsequent axes are ranked according to variance, with the final axis pointing in the direction of the lowest variance [23].

The magnetometer is placed inside the 3-D Helmholtz coil. First, all the magnetometer parameters are set to initial values. The initial direction of the magnetic field is induced by the coil and then in opposite direction. During the measurements, the magnetic field is stationary and homogenous. The magnetometer acquires two measurements (in the initial direction and the opposite direction) and these measurements are used in the UKF algorithm to update the initial values of the parameters with new estimated values. The subsequent direction of the magnetic field vector of the coil for the next instance of measurements for the set of measurements needed for calibration is calculated from the singular vector $\mathbf{u}_1$. This singular vector $\mathbf{u}_1$ corresponds to the principle axis with the highest variance expressed in the coordinate frame of the magnetometer. The algorithm calculates the direction of the magnetic field in the direction of the largest variance of the estimated parameters. Then, the sensor takes measurements of the magnetic field in the calculated direction and also in the opposite direction. Thus, the sensor measures the magnetic field in both directions where the variance of the estimated parameters is highest. Then, after the new set of measurements of the magnetic field has been taken, the parameters are updated. With each new update of the estimated sensor parameters, a new direction of the magnetic field is also computed and applied by the 3-D Helmholtz coil to reduce the variance along the axis with largest uncertainty. The final result is a sequence of magnetic field directions, which subsequently maximize the sensitivity of the parameter with largest variance.

E. Simulation and Measurements

Simulation is used to verify the kinematic model and the proposed procedure, since the true parameters of the real sensor are not known. In the simulation, all sensor parameters are manually predefined in the kinematic model of the magnetic sensor and are later compared with the simulation results. The simulation is built and run in MATLAB. The simulation is organized into three parts. First, the data from the magnetometer are acquired (in simulation, the values are calculated using the initially predefined parameters), then the sensor output is fed into the UKF algorithm. The outputs of the UKF algorithm are estimated parameters and the magnetic field orientation for the next measurement. The last part is the changing of the direction of the magnetic field for the next parameter estimation.

Each simulation has a fixed number of 15 measuring/calibrating iterations. Since the model of the sensor and the UKF algorithm have a fixed noise parameter, different simulation runs produce different sensor outputs and parameter estimates. The scattering of the parameter values around the true predefined value can be used to evaluate the calibration method.

In the same way as for the simulation, multiple calibration runs are performed using a real three-axial magnetometer to evaluate the calibration method by comparing the estimated sensor parameters of the magnetometer between calibration runs. The magnetometer is placed in a 3-D Helmholtz coil that is controlled by a computer running the calibration method.

III. Result

A. Simulation Results

The evaluation is carried out by comparing the errors between the estimated parameters and the predefined parameters using three different calibration approaches. The first approach uses the proposed adaptive calibration method with the determination of magnetic field orientation for optimal parameter estimation. The second approach uses the UKF parameter estimation method with random predefined orientations of the magnetic field. The third approach uses manually chosen predefined orientations of the magnetic field in such a manner that all three sensor axes are sequentially covered with the magnetic field in both directions, including different combinations where all three sensor axes together are excited by the magnetic field. The simulation enables the determination of the parameters' estimation errors. Since the sensor parameters are predefined in the mathematical model that is used in the simulation, the estimated parameters that are the result of the calibration can be compared with the predefined parameters. The errors of parameter estimation are determined by running 100 simulation runs. Each simulation run has different randomly chosen sensor parameters that are used in

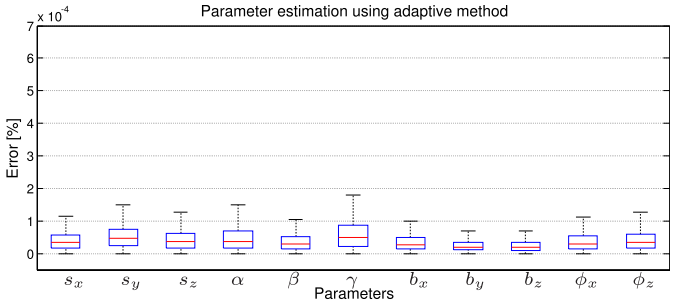

Fig. 2. Scatter of gain, misalignment, bias, and orientation parameters errors using adaptive method calibration. The middle line, the bottom, and the top of the box represent the median, the 25th and the 75th percentiles, respectively. The whiskers represent the furthermost value in the 1.5 interquartile ranges.

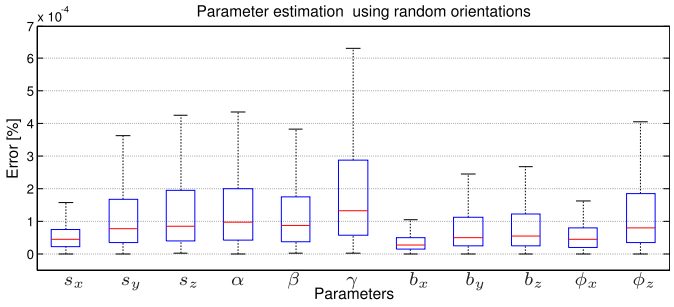

Fig. 3. Scatter of gain, misalignment, bias, and orientation parameters errors using the calibration method with random predefined magnetic field orientations. The middle line, the bottom, and the top of the box represent the median, the 25th, and the 75th percentiles, respectively. The whiskers represent the furthermost value in the 1.5 interquartile ranges. Outliers that occurred are not represented in this figure.

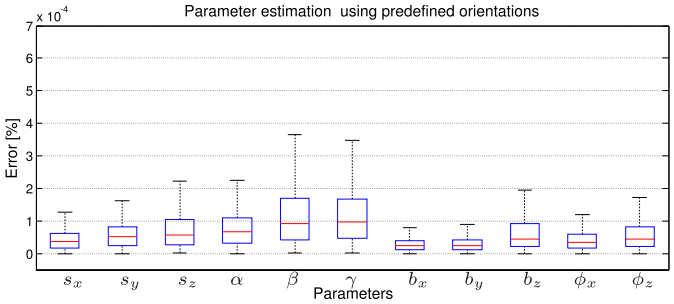

Fig. 4. Scatter of gain, misalignment, bias, and orientation parameters errors using the calibration method with manually predefined magnetic field orientations. The middle line, the bottom, and the top of the box represent the median, the 25th, and the 75th percentiles, respectively. The whiskers represent the furthermost value in the 1.5 interquartile ranges.

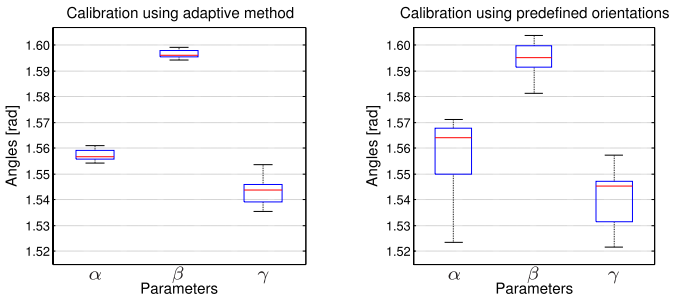

Fig. 5. Left plot presents the dispersion of misalignment parameters using the adaptive calibration method and the right plot presents the dispersion of the misalignment parameters using predefined magnetic field orientations. The dispersion is based on 10 calibration runs. In both plots, the middle line represents the median, and the bottom and the top of the box represent the 25th and 75th percentiles, respectively. The whiskers represent the furthermost value in the 1.5 interquartile ranges.

the mathematical model of the sensor. The gain parameters are in the range 0.9–1.1, the misalignment parameters are in the range 1.52–1.62 rad, the bias parameters are in the range −6–6 μT, and the orientation parameters are in the range −0.1–0.1 rad. Each simulation run consists of 1000 calibration runs. The calibration outputs are stored and used for statistical analysis.

Fig. 2 shows the distribution of the error difference between preset and estimated parameters for gain, misalignment, bias, and orientation. The data are gathered by simulating the adaptive calibration method, where the orientations of the magnetic field are determined automatically. The middle line of each box represents the median value, the bottom and the top of the box present the 25th and 75th percentiles, and the whiskers represents the furthermost value in the 1.5 interquartile ranges.

Similarly to the previous figure, Fig. 3 shows the error distribution of the estimated parameters where the data are gathered by simulating the calibration method using random predefined orientations of the magnetic field. Since some combinations of random orientations are not suitable to successfully estimate sensor parameters, higher errors (up to 0.035%) occur. Higher errors are not represented in this figure in order to achieve a better comparison between methods.

The errors of parameters estimation determined by using the simulation of calibration with manually predefined orientations of magnetic field are shown in Fig. 4. The middle line of each box represents the median value, the bottom and the top of the box represent the 25th and 75th percentiles, and the whiskers represent the furthermost value in the 1.5 interquartile ranges.

B. Real Magnetometer Results

Evaluation of the calibration method is also performed by using the real magnetometer in a 3-D Helmholtz coil with compensation of the outer magnetic field. The coil is set to induce a magnetic field in any direction that the calibration method calculates with an amplitude of 40 μT. Since the actual sensor parameters are unknown, the evaluation can be carried out by comparing the results of ten calibration runs of the same magnetometer using the adaptive calibration method and ten calibration runs with predefined magnetic field orientations. The method with random magnetic field orientations is excluded due to the inaccuracy of the parameters estimation.

Fig. 5 shows the output of misalignment parameter estimation for ten calibrations of the same magnetometer. The left subfigure presents data obtained from the adaptive calibration method, while the right subfigure presents data obtained from the calibration method with manually predefined magnetic field orientations. The middle line of each box represents the median value, the bottom and the top of the box represent the 25th and 75th percentiles, and the whiskers represent the furthermost value in the 1.5 interquartile ranges. The output values of bias and gain parameters obtained by both calibration methods are presented in Table I.

TABLE I

CALIBRATION RESULTS OF ESTIMATING PARAMETERS GAIN AND BIAS USING THE PROPOSED CALIBRATION METHOD AND THE CALIBRATION METHOD WITH PREDEFINED ORIENTATIONS. THE FIRST COLUMN REPRESENTS MINIMUM VALUES, THE SECOND COLUMN REPRESENTS THE 25TH PERCENTILE, THE THIRD COLUMN REPRESENTS MEDIAN VALUES, THE FOURTH REPRESENTS THE 75TH PERCENTILE, AND THE LAST COLUMN REPRESENTS THE MAXIMUM VALUES OF ESTIMATED PARAMETERS

		min	25th	median	75th	max
Calibration with adaptive determined orientations						
gain	x	1.037	1.041	1.044	1.045	1.047
	y	1.032	1.036	1.036	1.038	1.039
	z	0.970	0.973	0.974	0.976	0.977
bias [μT]	x	11.380	11.456	11.800	11.932	12.008
	y	-4.224	-4.272	-4.380	-4.428	-4.552
	z	0.408	0.488	0.544	0.592	0.652
Calibration with manually predefined orientations						
gain	x	1.044	1.046	1.047	1.048	1.051
	y	1.020	1.032	1.037	1.042	1.052
	z	0.967	0.970	0.973	0.973	0.975
bias [μT]	x	11.892	11.792	11.812	11.848	11.868
	y	-3.976	-4.296	-4.440	-4.624	-4.788
	z	0.216	0.400	0.468	0.528	0.708

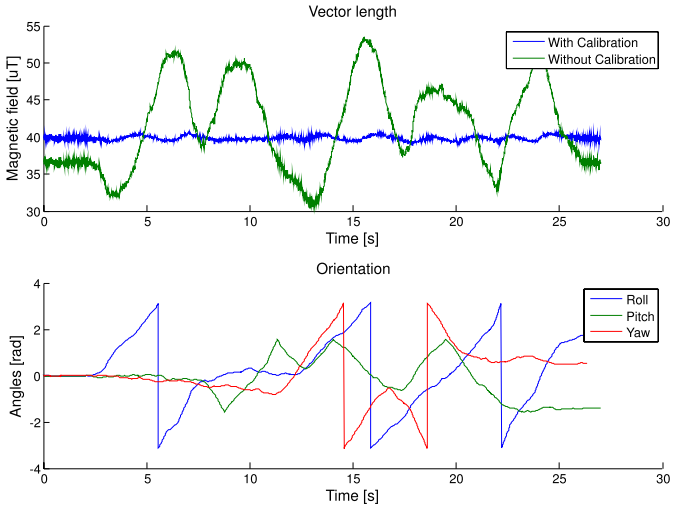

Fig. 6. Upper plot represents measurements of the constant magnetic field during manual rotation of the magnetometer. The green line represents sensor output before calibration and the blue line represents sensor output after calibration. The lower plot represents the orientation of the sensor calculated from the on-board gyroscope.

The estimated parameters of the real magnetometer are further evaluated by observing the magnitude of the magnetic field measured by all three axes of the magnetometer before and after the calibration. The Helmholtz coil is set to create a constant magnetic field of 40 μT in a Z-direction of the coil. The magnetometer is rotated by hand in the center of the coil where the field uniformity is within 1% [24]. The upper part of Fig. 6 shows the output of the magnetometer before and after calibration. The lower part of Fig. 6 shows the orientation of the sensor obtained from the on-board gyroscope. The orientation calculated using the gyroscope was added for illustrative purposes, to show that the unit has been rotated around all axes.

In the next test, the comparison between parameters obtained by the proposed adaptive method and the method with predefined orientations is done with the same conditions as the previous comparison, except that the magnetometer is attached to a plastic cube and placed in six different orientations marked in Fig. 7 while the measurements of the magnetic field are observed using calibration data obtained from both methods. Fig. 7 shows the output of the magnetometer with the blue line representing the output of the magnetometer with parameters obtained with the adaptive calibration method, and the green line representing the output of the magnetometer after calibration with the calibration method with the predefined orientations. Calibration of 40 magnetometers of the same type shows that the range of gain parameters is 0.9–1.1, the range of misalignment parameters is 1.5–1.6 rad, and the range of bias parameters is -16–16 μT.

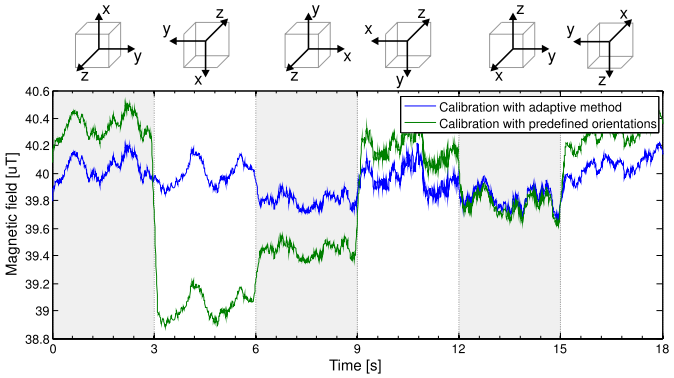

Fig. 7. Lower plot presents measurements of the constant magnetic field while the magnetometer is placed in six different orientations using a cube. The blue line represents the magnetometer output after calibration with the adaptive calibration method and the green line represents the magnetometer output after calibration with the calibration method that uses predefined orientations. The upper figure presents informative orientations of the magnetometer.

IV. DISCUSSION

The comparison of results presented in Figs. 2–4 shows that the calibration method with random predefined orientations (Fig. 3) of the magnetic field generally yields the highest error of the estimation of the magnetometer parameters. Due to the low number of iterations, the random orientations of the magnetic field are not sufficient for successful parameters estimation. In some cases where subsequent orientations do not differ enough from each other, errors can be significantly higher, up to 0.035%. These higher error values are not shown in Fig. 2 to maintain the same scale of the plots for better comparison of the methods. The results also show that the median values of parameter estimation errors of the method using random orientations are higher, compared with the proposed adaptive calibration method.

A smaller difference in median values of what is observed between the adaptive calibration method and the calibration method with predefined orientations is shown in Fig. 4. This can be expected, since the predefined orientations are selected in such a manner that each of the sensor axes is exposed to the magnetic field in both directions, which should lead to enough measurements to accurately estimate the magnetometer parameters. However, the sensor is not always perfectly aligned with the axes of the magnetic coil,

which results in a lower effectiveness of parameters estimation. Thus, higher errors can occur in parameters estimation, which can be seen in Fig. 4, especially in the estimation of gain and misalignment parameters. Based on simulation results, it can be concluded that the adaptive calibration method can estimate sensor parameters more accurately, due to the ability to calculate the optimum magnetic field orientations for the given placement of the magnetometer inside the coil and the estimate effect of the nonidealities of the given magnetometer on the output of the sensor. The median values of the parameters errors are the lowest in the proposed adaptive method compared with the other two methods. Furthermore, the maximum parameter errors are, in general, the lowest in the adaptive calibration method.

The simulation results show that both the adaptive method and the method with predefined orientations can deliver satisfactory results. Both methods are therefore tested on a real magnetometer using a 3-D Helmholtz magnetic coil. Fig. 5 shows that dispersion of the estimated misalignment error of a real magnetometer is lower with the adaptive method. The bias and gain parameters presented in Table I also have lower dispersion when using the adaptive method. Results obtained from the real magnetometer correspond to the simulation results with the observation that magnitude of the errors is higher. Considering that the calibration methods are simulated in ideal conditions, the difference in magnitude of errors is expected. The real system consists of a reference magnetometer and a control system that controls the magnetic coils and compensates for the external magnetic field. The main contributor to the errors in real calibration is the dynamically changing external magnetic field that cannot be compensated by the magnetic coil [16].

The results shown in Fig. 7 demonstrate the influence of the parameter estimation dispersion on the magnetometer output. If the sensor parameters were perfectly estimated, the output of sensor in the constant magnetic field would be constant regardless of the sensor orientation.

Fig. 7 shows that the output of the magnetometer varies in the range of 0.2 μT when it is placed in different orientations. This difference is even larger in the case of sensor parameters obtained from the calibration exploiting predefined orientations. In the same figure can be seen the variation of the magnetic field during experimental time, especially in the last sensor orientation, when the output changes from 39.9 to 40.2 μT even though the sensor is stationary, and the coil closed loop control is set to induce a constant magnetic field.

However, the output of the magnetometer is unusable without highly precise calibration (Fig. 6). In this case, the output changes by more than 17 μT, depending on the orientation of the magnetometer. In the same figure, it can be also seen that the output of the calibrated sensor is constant, taking into account that the coil can compensate for the dynamical magnetic disturbances.

The results show an advantage of the proposed adaptive calibration method in parameter estimation. With only 15 iterations, the estimation error using the adaptive calibration method is lower compared with the calibration method with predefined orientations. Since the optimal magnetometer calibration orientations are determined online by the adaptive calibration method, there is no need to manually interfere, set, adjust, or orient the magnetic field to the appropriate value, as this is automatic and shortens the time of calibration. In contrast to the method presented in [25], a large number of samples must be acquired to obtain satisfactory results. Special equipment must also be used to manually determine different sensor orientations and some precautions must be taken to ensure that magnetic field stays constant during calibration. Although calibration method presented in [26] achieves higher accuracy in parameter estimation, it also requires a large number of samples and more processing time. On the other hand, the disadvantage of this method is use of relatively expensive equipment for magnetic field orientation. While the method described in [27] does not require any special equipment or reference information it still requires sufficient number of random sensor orientations that are set manually.

The equipment setup for the proposed method includes the reference magnetometer used in the coil and a controller for controlling the magnetic field produced by the coil. The reference magnetometer must be more accurate and should be calibrated with traceability to the higher standards. The system must also be able to compensate for external magnetic fields together with any dynamic deviations of the magnetic field due to external disruptions.

V. Conclusion

This paper presents an online adaptive calibration method for a three-axial magnetometer. A 3-D Helmholtz coil is used to create a number of different orientations of the magnetic field inside the coil. A UKF estimates three main magnetometer parameters (gain, misalignment, and bias) in an online algorithm during the calibration. The subsequent orientations of the magnetic field to which the calibrated magnetometer are exposed and are automatically calculated during the calibration procedure, using the output covariance to estimate the next optimal orientation of the magnetic field for parameter estimation.

An evaluation of the proposed adaptive method was performed using simulation and real measurements in the 3-D Helmholtz coil. High accuracy was achieved and demonstrated after a low number of 15 iterations. The results from the adaptive approach were compared with the results obtained with the calibration method where magnetic field orientations were predefined. Although the offline calibration method with a higher number of iterations could achieve higher accuracies, this paper represents a method that can automatically determine appropriate magnetic field orientations for calibration and thus rapidly produce sufficiently accurate sensor parameters using a low number of iterations.

References

[1] R. Mayagoitia, A. Nene, and P. Veltink, "Accelerometer and rate gyroscope measurement of kinematics: An inexpensive alternative to optical motion analysis systems," *J. Biomech.*, vol. 35, no. 4, pp. 537–542, 2002.

[2] J. Včelàk, P. Ripka, J. Kubik, A. Platil, and P. Kašpar, "AMR navigation systems and methods of their calibration," *Sens. Actuators A, Phys.*, vol. 123, pp. 122–128, Nov. 2005.

[3] E. Bachmann, I. Duman, U. Usta, R. McGhee, X. Yun, and M. Zyda, "Orientation tracking for humans and robots using inertial sensors," in *Proc. IEEE Int. Symp. CIRA*, Nov. 1999, pp. 187–194.
[4] M. Mihelj, "Inverse kinematics of human arm based on multisensor data integration," *J. Intell. Robot. Syst.*, vol. 47, no. 2, pp. 139–153, 2006.
[5] Z.-Q. Zhang, X.-L. Meng, and J.-K. Wu, "Quaternion-based Kalman filter with vector selection for accurate orientation tracking," *IEEE Trans. Instrum. Meas.*, vol. 61, no. 10, pp. 2817–2824, Oct. 2012.
[6] S. Bonnet, C. Bassompierre, C. Godin, S. Lesecq, and A. Barraud, "Calibration methods for inertial and magnetic sensors," *Sens. Actuators A, Phys.*, vol. 156, no. 2, pp. 302–311, 2009.
[7] F. Camps, S. Harasse, and A. Monin, "Numerical calibration for 3-axis accelerometers and magnetometers," in *Proc. IEEE Int. Conf. Electro/Inf. Technol.*, Jun. 2009, pp. 217–221.
[8] J. Wang, Y. Liu, and W. Fan, "Design and calibration for a smart inertial measurement unit for autonomous helicopters using MEMS sensors," in *Proc. IEEE Int. Conf. Mechatron. Autom.*, Jun. 2006, pp. 956–961.
[9] D. Campolo, M. Fabris, G. Cavallo, D. Accoto, F. Keller, and E. Guglielmelli, "A novel procedure for in-field calibration of sourceless inertial/magnetic orientation tracking wearable devices," in *Proc. 1st IEEE/RAS-EMBS Int. Conf.*, Feb. 2006, pp. 471–476.
[10] V. Petrucha, P. Kaspar, P. Ripka, and J. M. Merayo, "Automated system for the calibration of magnetometers," *J. Appl. Phys.*, vol. 105, no. 7, p. 07E704, 2009.
[11] E. Renk, M. Rizzo, W. Collins, F. Lee, and D. Bernstein, "Calibrating a triaxial accelerometer-magnetometer-using robotic actuation for sensor reorientation during data collection," *IEEE Control Syst. Mag.*, vol. 25, no. 6, pp. 86–95, Dec. 2005.
[12] R. L. Mcpherron and R. C. Snare, "A procedure for accurate calibration of the orientation of the three sensors in a vector magnetometer," *IEEE Trans. Geosci. Electron.*, vol. 16, no. 2, pp. 134–137, Apr. 1978.
[13] H. E. Soken and C. Hajiyev, "UKF-based reconfigurable attitude parameters estimation and magnetometer calibration," *IEEE Trans. Aerosp. Electron. Syst.*, vol. 48, no. 3, pp. 2614–2627, Jul. 2012.
[14] L. Bartolomeo, Z. Lin, S. Sessa, M. Zecca, H. Ishii, and A. Takanishi, "Online magnetic calibration of a cutting edge 9-axis wireless inertial measurement unit," *Int. J. Appl. Electromagn. Mech.*, vol. 39, no. 1, pp. 779–785, 2012.
[15] T. Beravs, P. Rebersek, D. Novak, J. Podobnik, and M. Munih, "Development and validation of a wearable inertial measurement system for use with lower limb exoskeletons," in *Proc. 11th IEEE-RAS Int. Conf. Humanoid Robot.*, Oct. 2011, pp. 212–217.
[16] S. Begus, M. Stanonik, and D. Fefer, "Stabilizacija magnetnega polja v 3D helmholtz tuljavi," in *Proc. 21st Int. Electrotech. Comput. Sci. Conf.*, 2012, pp. 185–188.
[17] D. Jurman, M. Jankovec, and R. Kamnik, "Calibration and data fusion solution for the miniature attitude and heading reference system," *Sens. Actuators A, Phys.*, vol. 138, no. 2, pp. 411–420, 2007.
[18] R. Van Der Merwe, "Sigma-point Kalman filters for probabilistic inference in dynamic state-space models," Ph.D. dissertation, OGI School Sci. Eng. Oregon Health, Sci. Univ., Beaverton, OR, USA, 2004.
[19] J. Ambadan and Y. Tang, "Sigma-point Kalman filter data assimilation methods for strongly nonlinear systems," *J. Atmos. Sci.*, vol. 66, no. 2, pp. 261–285, 2009.
[20] M. VanDyke, J. Schwartz, and C. Hall, "Unscented Kalman filtering for spacecraft attitude state and parameter estimation," Ph.D. dissertation, Dept. Aerosp. Ocean Eng., Virginia Polytechnic Inst. State Univ., Blacksburg, VA, USA, 2004.
[21] T. Beravs, J. Podobnik, and M. Munih, "Three-axial accelerometer calibration using Kalman filter covariance matrix for online estimation of optimal sensor orientation," *IEEE Trans. Instrum. Meas.*, vol. 61, no. 9, pp. 2501–2511, Sep. 2012.
[22] A. T. Nelson and E. A. Adviser-Wan, *Nonlinear Estimation and Modeling of Noisy Time Series by Dual Kalman Filtering Methods*. Hillsboro, OR, USA: Oregon Graduate Inst. Sci. Technol., 2000.
[23] C. Bishop and S. S. Enligne, *Pattern Recognition and Machine Learning*, vol. 4. New York, NY, USA: Springer-Verlag, 2006.
[24] E. L. Bronaugh, "Helmholtz coils for calibration of probes and sensors: Limits of magnetic field accuracy and uniformity," in *Proc. IEEE Int. Symp. Electromagn. Compat. Symp. Rec.*, Aug. 1995, pp. 72–76.
[25] F. Hoflinger, J. Muller, R. Zhang, L. Reindl, and W. Burgard, "A wireless micro inertial measurement unit (IMU)," *IEEE Trans. Instrum. Meas.*, vol. 62, no. 9, pp. 2583–2595, Sep. 2013.
[26] Z. Wu, Y. Wu, X. Hu, and M. Wu, "Calibration of three-axis magnetometer using stretching particle swarm optimization algorithm," *IEEE Trans. Instrum. Meas.*, vol. 62, no. 2, pp. 281–292, Feb. 2013.
[27] J. Fang, H. Sun, J. Cao, X. Zhang, and Y. Tao, "A novel calibration method of magnetic compass based on ellipsoid fitting," *IEEE Trans. Instrum. Meas.*, vol. 60, no. 6, pp. 2053–2061, Jun. 2011.

Tadej Beravs received the B.Sc degree from the Faculty of Electrical Engineering, University of Ljubljana (UL), Ljubljana, Slovenia, in 2010.

He is currently a Junior Researcher and Ph.D. Student with the Laboratory of Robotics, UL. His current research interests include calibration methods and development of inertial measurement units.

Samo Beguš received the B.Sc., M.Sc., and Ph.D. degrees in electrical engineering from the University of Ljubljana, Ljubljana, Slovenia, in 2001, 2004, and 2007, respectively.

His current research interests include electrical measurements, precision magnetic measurements, sensor systems, audio signal processing, and audio measurements.

Janez Podobnik received the B.Sc degree in electrical engineering and the Ph.D. degree from the University of Ljubljana (UL), Ljubljana, Slovenia, in 2004 and 2009, respectively.

He is currently a Researcher and Teaching Assistant with UL. His current research interests include haptic interfaces, real-time control of robots for virtual-reality-supported rehabilitation, and sensory fusion techniques.

Marko Munih (M'88) received the Ph.D. degree in electrical engineering from the University of Ljubljana (UL), Ljubljana, Slovenia.

He is currently a Full Professor and Head of the Laboratory of Robotics and was the Head of the Department for Measurements and Process Control, Faculty of Electrical Engineering, UL, from 2004 to 2006. He was a principal investigator on eight EU projects. His research focuses on robot contact with environment, as well as construction and use of haptic interfaces in the fields of industry and rehabilitation engineering, in combination with virtual reality. His expertise includes applications in construction and robots for measurement tasks. His current research interests include functional electrical stimulation of paraplegic lower extremities with surface electrode systems, including measurements, control, biomechanics, and electrical circuits.